

# A pulsed-power implementation of “Laser Gate” for increasing laser energy coupling and fusion yield in Magnetized Liner Inertial Fusion (MagLIF)

S. M. Miller,<sup>1, a)</sup> S. A. Slutz,<sup>2</sup> S. N. Bland,<sup>3</sup> S. R. Klein,<sup>1</sup> P. C. Campbell,<sup>1</sup> J. M. Woolstrum,<sup>1</sup> C. C. Kuranz,<sup>1</sup> M. R. Gomez,<sup>2</sup> N. M. Jordan,<sup>1</sup> and R. D. McBride<sup>1</sup>

<sup>1)</sup>*Nuclear Engineering and Radiological Sciences, University of Michigan, Ann Arbor, MI 48109, USA*

<sup>2)</sup>*Sandia National Laboratories, Albuquerque, NM 87185, USA*

<sup>3)</sup>*Department of Physics, Imperial College London, London SW7 2BW, UK*

(Dated: 26 May 2020)

Magnetized Liner Inertial Fusion (MagLIF) at Sandia National Laboratories involves a laser preheating stage, where a few-ns laser pulse passes through a few-micron-thick plastic window to preheat gaseous fusion fuel contained within the MagLIF target. Interactions with this window reduce heating efficiency and mix window and target materials into the fuel. A recently proposed idea called “Laser Gate” involves removing the window well before the preheating laser is applied. In this article, we present experimental proof-of-principle results for a pulsed-power implementation of Laser Gate, where a thin current-carrying wire weakens the perimeter of the window, allowing the fuel pressure to push the window open and away from the preheating laser path. For this effort, transparent targets were fabricated and a test facility capable of studying this version of Laser Gate was developed. A 12-frame bright-field laser schlieren/shadowgraphy imaging system captured the window opening dynamics on microsecond timescales. The images reveal that the window remains largely intact as it opens and detaches from the target. A column of escaping pressurized gas appears to prevent the detached window from inadvertently moving into the preheating laser path.

## I. INTRODUCTION

One approach to inertial confinement fusion (ICF) in the laboratory is Magnetized Liner Inertial Fusion (MagLIF).<sup>1,2</sup> This concept is being tested experimentally on the Z pulsed-power facility at Sandia National Laboratories (SNL).<sup>3-5</sup>

MagLIF can be described by the three-step process illustrated in Fig. 1. A MagLIF target consists of a cylindrical metal tube (or “liner”) surrounded by vacuum and filled with fusion fuel (e.g., pressurized deuterium or deuterium-tritium gas). During the first stage of MagLIF, the entire target (including both the liner and the fuel) is premagnetized with an axial magnetic field. This is done to thermally insulate the hot fuel from the cold liner wall during the implosion. This is also done to trap charged fusion products in the fuel during peak compression, so that the charged products deposit their kinetic energy back into the fuel for self-heating (e.g., self-heating from  $\alpha$  particles when deuterium-tritium fusion events occur). Note that the axial field is amplified via magnetic flux compression during the implosion phase. This amplification allows the field to thermally insulate the fuel even as the fuel becomes increasingly hot and the radial extent of the fuel becomes increasingly small.

During MagLIF’s preheating stage (which occurs just as the fuel begins to implode), a few-ns, multi-kJ laser pulse deposits energy into the pressurized fuel. This raises the fuel temperature to  $\sim 100$  eV.

During the implosion stage, the Z facility’s current pulse, which rises from 0 to approximately 20 MA in

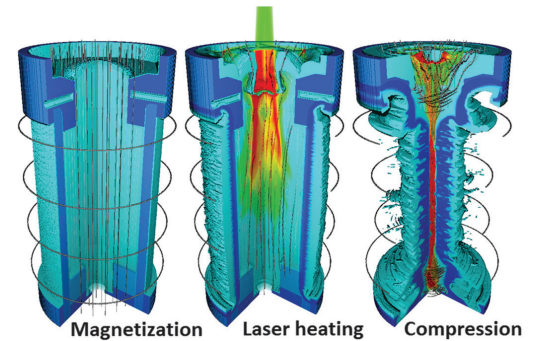


FIG. 1. A schematic representation of the three phases of MagLIF. An axial current generates an azimuthal magnetic field, which is used to implode a gas-filled cylindrical target that is premagnetized with an axial field. Near the start of the implosion, the fuel is heated by the Z-Beamlet laser. The liner compresses and further heats the fuel to fusion-relevant temperatures and densities at stagnation. Reprinted figure with permission from M. R. Gomez *et al.*, *Phys. Rev. Lett.*, **113**, 155003, (2014). Copyright 2014 by the American Physical Society.<sup>3</sup>

100 ns, flows axially along the liner’s outermost surfaces. This generates an azimuthal magnetic field that surrounds the liner and a corresponding intense magnetic pressure that drives the liner radially inwards. The imploding liner does adiabatic “ $PdV$ ” work on the hot, magnetized fuel. This both compresses and further heats the fuel to fusion relevant temperatures ( $>2$  keV) and densities ( $>0.2$  g/cm<sup>3</sup>).<sup>1,3</sup>

MagLIF target designs feature a laser entrance hole (LEH) covered by a thin (few-micron-thick) window to hold the pressurized fuel in place (see Fig. 2). This win-

<sup>a)</sup>Corresponding author: smmil@umich.edu

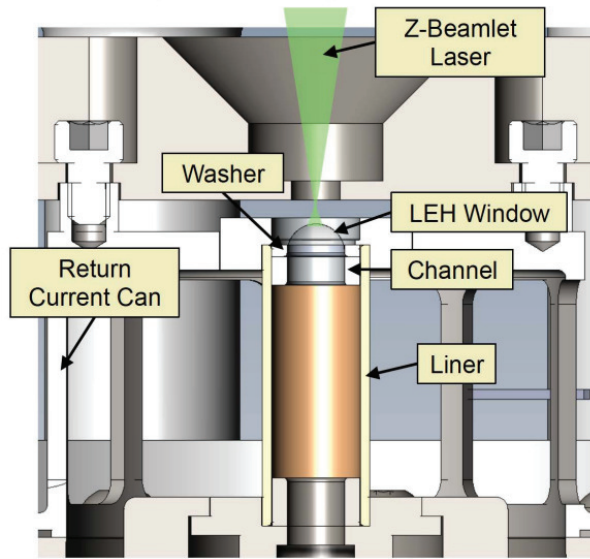


FIG. 2. An illustration of the MagLIF target chamber area showing the preheating laser (Z-Beamlet) illuminating the LEH window from above the fuel-containing liner target.

dow is nominally transparent; however, the high intensity laser causes the window material to ablate and ionize, which leads to laser plasma instabilities (LPI). Energy losses are believed to occur because of this LPI, energy absorption into the window material, and from window material mixing into the fuel (which leads to enhanced radiation loss).<sup>5-10</sup> To reduce these losses, the LEH window could be removed before the preheating laser passes through the LEH. This concept of early-time window removal is referred to as “Laser Gate”.<sup>4</sup>

There are presently two implementations of Laser Gate being explored. One implementation,<sup>4</sup> which is being tested at SNL,<sup>11</sup> uses an auxiliary laser pulse to remove the window early in time. This auxiliary pulse has a beam spatial profile in the shape of a six-pronged asterisk. When this auxiliary pulse is applied to the LEH window, the window material is weakened/broken in the shape of the beam’s spatial profile, which allows the pressurized fuel to push the window open like a flower opening with six petals. The subsequent preheating pulse (Z-Beamlet) is then free to enter the fuel region without interacting with these blown-open window petals.

Another implementation of Laser Gate, which has now been tested at the University of Michigan (UM) and is the subject of this paper, uses a current pulse to heat a wire wrapped around the perimeter of the LEH window (see Fig. 3). The heated wire melts/weakenes the window material that the wire is in contact with, thus cutting/breaking the window attachment to the target in a controlled fashion. This then allows the pressurized fuel to push the window open and out of the laser path. The subsequent preheating laser pulse (Z-Beamlet) would be timed to enter the LEH after the window has fully opened and is no longer an obstruction. As shown

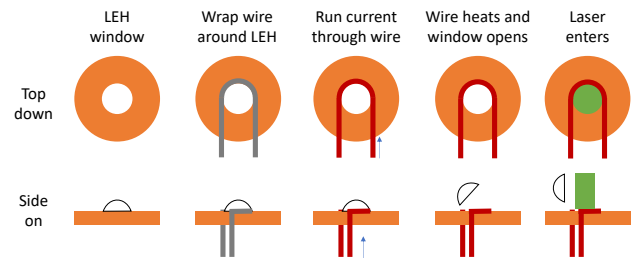


FIG. 3. Pulsed-power implementation of the Laser Gate concept, where electrical current is driven through a wire to remove the LEH window from the preheating laser path. Both top-down and side-on views are presented.

in Fig. 3, the wire is in contact with only about half of the LEH window perimeter. This allows the window opening direction to be controlled by creating a hinge for the window to open along. Ideally, the window material would stay hinged to the target so that the window is not free to move about and potentially interfere with the preheating laser or other equipment. When integrated with MagLIF experiments, this pulsed-power implementation of Laser Gate should lead to reduced LPI, reduced energy losses due to absorption in the window material, and reduced radiative losses due to fuel-window mix.

Besides MagLIF, the Laser Gate concept could, in principle, be applied to other ICF programs as well. For example, Laser Gate could be used to remove the LEH windows from the hohlraums that surround the ICF targets on the National Ignition Facility (NIF).<sup>12,13</sup> The LEH windows and gas-fill densities used for the NIF hohlraums are fairly similar to those used for MagLIF targets. However, a more detailed cost-benefit analysis would be required to assess whether or not Laser Gate on the NIF would be useful and practical.

The remainder of this paper is organized as follows. In Sec. II, the Laser Gate targets are characterized. In Sec. III, the facility developed to test the Laser Gate targets is described. This facility consists of a small current pulser and imaging diagnostics. In Sec. IV, experimental results (images) are presented. In Sec. V, conclusions are summarized and future work is discussed.

## II. TARGET DESIGN AND FABRICATION

The targets for these studies were designed and fabricated at UM (see Fig. 4). Their dimensions were chosen to be similar to the dimensions of the MagLIF targets tested on the Z facility at SNL (see Table I for comparisons). The UM target bodies were all 25 mm tall. They were made from transparent acrylic tubing to allow visible diagnostic access to the gas dynamics occurring inside the targets. The tubing was chosen to be square in cross section (flat on the sides) to better enable side-on laser probing techniques (e.g., side-on bright-field schlieren/shadowgraphy imaging). Note that the work

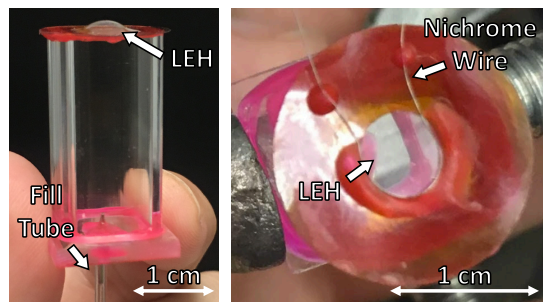


FIG. 4. UM target for testing Laser Gate. When pressurized, the window material stretches out into the domed shape shown on the left. Shown on the right is the nichrome wire attached to about half of the LEH perimeter.

TABLE I. Comparison of UM and SNL target parameters. The timescales were calculated using Eqs. 1 and 2.

Target Parameters	Laser-Gate Targets (UM)	MagLIF Targets (SNL)
Gas Type	Air	Deuterium
Window Thickness ( $\mu\text{m}$ )	3	1.6
Window Radius (mm)	2.6	1.1
Pressure Difference (atm/psi)	2/30	8/120
Window Material	Mylar	Polyimide
Window Density ( $\text{g}/\text{cm}^3$ )	1.38	1.42
Beveled Washer	No	Yes
Ambient Pressure	Atmosphere	Vacuum
Sound Speed (m/s)	343	924
Target Length (mm)	25	12
Opening Time, $\tau_{\text{open}}$ ( $\mu\text{s}$ )	14.3	3.4
Evacuation Time, $\tau_{\text{evac}}$ ( $\mu\text{s}$ )	74.1	13.0
Ratio $\tau_{\text{open}}/\tau_{\text{evac}}$	0.19	0.26

presented in this article does not include a study of the internal gas dynamics, but these targets were designed to enable such experiments in the future.

Each target body (each transparent acrylic tube) was capped on the top with the LEH and on the bottom with another piece of acrylic to hold the gas fill tube in place. The LEH was made from an orange polyimide washer. The washer was 0.15 mm thick, with an inner diameter of 5.16 mm and an outer diameter of 15.9 mm. The LEH window was made from 3- $\mu\text{m}$ -thick Mylar. The targets were assembled using glue that was cured by ultraviolet light. A nichrome wire (80% Ni, 20% Cr) of 100- $\mu\text{m}$  diameter was glued down to one half of the inner perimeter of the washer (see Fig. 4). The LEH window was then glued to the underside of the polyimide washer. When these targets were pressurized, the window material would stretch and form the domed shape shown in Fig. 4. When the window material bubbles out, it makes contact with the nichrome wire around the washer.

To pressurize the targets, a calibrated gas-fill system was used. This system is capable of achieving up to 120 psig (8.2 atm). We used air instead of deuterium to fill the targets, because air is readily available and

does not require extra safety precautions.

It is important to note that SNL MagLIF experiments are done with the target surrounded by vacuum, while our UM Laser Gate experiments were done with the target surrounded by atmosphere. The important quantity governing the window opening dynamics is the pressure difference across the window,  $\Delta P$ . Thus, throughout this paper, the pressures will be stated in terms of  $\Delta P$  values.

In filling the targets, the goal was to use  $\Delta P$  values similar to the lower end of the  $\Delta P$  values used in MagLIF experiments at SNL (approximately 60 psi in Ref. 3); however, we were only able to reliably achieve  $\Delta P$  values of about 30 psi (2.0 atm). During our first attempts to pressurize to  $\Delta P = 60$  psi, the LEH windows broke consistently. MagLIF targets fabricated at SNL are capable of reaching  $\Delta P$  values of at least 120 psi (8.2 atm).<sup>14</sup> The premature breaking of the Mylar windows in the UM targets is thought to be due in part to the value of  $(\delta/r)^2$  that was used, where  $\delta$  is the window thickness and  $r$  is the window radius, and in part to the sharp corners on the inside lip of the washers that were used. The pressure a window is capable of holding before bursting is proportional to  $(\delta/r)^2$ . The  $(\delta/r)^2$  for an SNL target is 1.62 times larger than that of the UM targets, so the UM targets should only hold about 60% of the pressure of an SNL target. Additionally, the washers used in the construction of SNL targets are beveled on the edge that the LEH window material stretches around, thus eliminating the sharp corner. Future UM targets will use beveled washers and smaller LEH window radii to better match SNL's  $(\delta/r)^2$  value.

Analytic estimates were performed to compare the opening time of the LEH window to the time it would take for the fuel (gas) to evacuate the target. We modeled the LEH window as a rigid disk that hinges about one point on its perimeter, so the window opening time can be expressed in SI units as

$$\tau_{\text{open}} = \left(\frac{5\pi}{4}\right)^{1/2} \left(\frac{\rho_w \times \delta \times r}{\Delta P}\right)^{1/2}, \quad (1)$$

where  $\rho_w$  is the density of the window material,  $\delta$  is the thickness of the window,  $r$  is the radius of the window, and  $\Delta P$  is the difference in pressure between the target fuel and the ambient pressure surrounding the target. The pressure difference was assumed to be uniform and constant, and the window was considered open when it had rotated 90° from its original position.

The evacuation time was taken to be the amount of time needed for a rarefaction wave, moving at the speed of sound for the given fuel type and pressure, to reach the bottom of the target. This can be expressed in SI units as

$$\tau_{\text{evac}} = \left(\frac{L}{c_s}\right) = L \times \left(\frac{M}{\gamma RT}\right)^{1/2}, \quad (2)$$

where  $L$  is the length of the target body,  $c_s$  is the sound speed,  $M$  is the molar mass of the fuel (gas),  $\gamma$  is the

adiabatic constant of the fuel (gas),  $R$  is the universal gas constant, and  $T$  is the temperature of the fuel (gas). Both fill gases (air for the UM Laser Gate targets and deuterium for the SNL MagLIF experiments) were taken to be diatomic, so  $\gamma = 1.4$  was used. Additionally, the fuel temperature was set to room temperature.

Ideally, the evacuation time would be much longer than the window opening time, so that most of the fuel would still be inside the target when the window is fully opened and the preheating laser pulse is applied. For the UM targets,  $\tau_{\text{open}} \approx 14.3 \mu\text{s}$ , and  $\tau_{\text{evac}} \approx 74.1 \mu\text{s}$ . For the SNL targets,  $\tau_{\text{open}} \approx 3.4 \mu\text{s}$ , and  $\tau_{\text{evac}} \approx 13.0 \mu\text{s}$ . These comparisons and others are summarized in Table I. There are various MagLIF target designs that are fielded on the Z facility, but for the sake of comparison, only one set of design parameters was chosen (a set from a recent study at SNL<sup>15</sup>). For the SNL target chosen, the rarefaction wave will have propagated about one fourth of the way down the target by the time the window is fully open. However, in this sample set of target parameters, the laser entrance channel is 2 mm in height, while the imploding liner height is 10 mm (see Fig. 2). The rarefaction wave propagating at roughly the speed of sound will move about 3 mm into the target during the 3.4  $\mu\text{s}$  opening time. Therefore, the rarefaction wave will have propagated through the 2 mm laser entrance channel and only 1 mm (or about 10%) into the imploding fuel region throughout the opening time. This set of target parameters could be optimized by increasing the length of the laser entrance channel by 1 mm, so that the rarefaction wave arrives at the top of the imploding liner just after the window fully opens. Note, however, that any laser energy deposited in the gas escaping from the laser entrance channel is considered a loss of preheat energy, since this energy does not contribute to preheating the fuel in the imploding region of the target. If the laser entrance channel becomes too long, then this energy loss could become comparable to the energy losses associated with LPI and absorption in the LEH window material. To better understand where this transition occurs, detailed preheating studies are required. These studies will involve both simulations and experiments using the platform described in this paper.

Other possible solutions for reducing the ratio  $\tau_{\text{open}}/\tau_{\text{evac}}$  (based on Eqs. 1 and 2) could involve increasing the gas density or decreasing the window mass (density, radius, or thickness). However, some of these changes (e.g., window thickness) could also weaken the windows and thus reduce the fuel pressures that the targets/windows could hold. Therefore, care must be taken when evaluating such tradeoffs.

Finally, it is important to note that  $\tau_{\text{open}}$  and  $\tau_{\text{evac}}$  have the same temperature dependence (see Eqs. 1 and 2). Thus, the ratio  $\tau_{\text{open}}/\tau_{\text{evac}}$  is not a function of temperature. This means that Laser Gate could be implemented on a cryogenically cooled MagLIF target, which is important for future high-gain MagLIF designs<sup>16</sup>.

### III. EXPERIMENTAL TEST FACILITY

The experimental facility assembled at UM to test the Laser Gate concept included a small current pulser,<sup>17,18</sup> an iPhone 6s video camera, and a 12-frame bright-field laser schlieren/shadowgraphy imaging system (see Fig. 5). The pulser was used to drive current through the nichrome wire on the target. This pulser consisted of a 240-nF capacitor (charged to 13 kV), an atmospheric-pressure spark-gap switch, and a 0.83- $\Omega$  resistor array. The pulser was charged by a DC power supply capable of generating up to 20 kV. The voltage on the power supply was increased manually until the gas in the spark-gap switch broke down, closing the switch, and allowing electrical current to flow to the target. Preliminary testing showed that the electrical current driven through the nichrome wire was so high that the wire exploded. To reduce the current, an additional resistance of 50–60  $\Omega$  was added to the output of the pulser. The wire then remained intact while still being heated enough to melt/weaken the LEH window on the target. A Pearson coil was used to measure the current through the nichrome wire. Depending on the attached output resistor, the measured peak current had a range of 150–170 A. An example current trace is shown in Fig. 6.

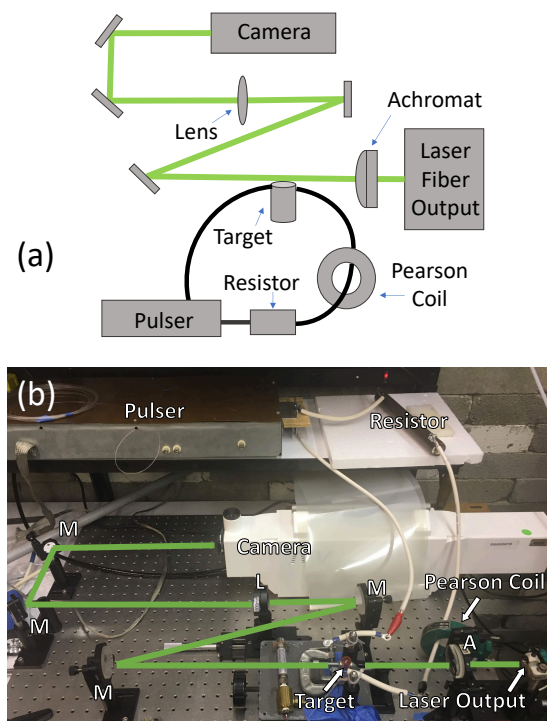


FIG. 5. (a) Block diagram of the bright-field laser schlieren/shadowgraphy imaging system coupled to the pulser-target system. (b) Photo of the experimental configuration used to acquire schlieren/shadowgraphy images. This setup includes a collimating achromat (A), mirrors (M), and a focusing lens (L).

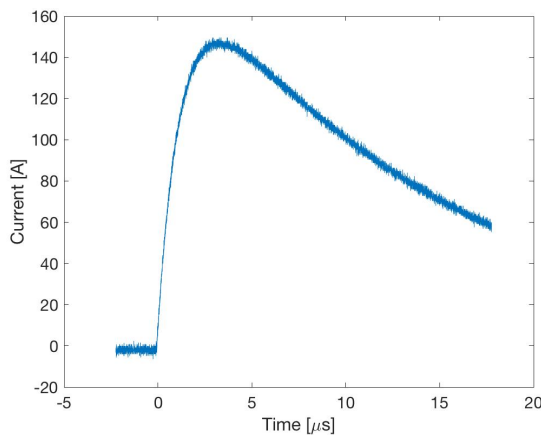


FIG. 6. Current pulse driven through the nichrome wire to melt/weaken the LEH window. This measurement was obtained using a Pearson coil.

The iPhone video camera was used to image the window opening dynamics on millisecond timescales. With the slow-motion feature enabled, this camera is capable of recording up to 240 fps (a frame spacing of about 4 ms).

The 12-frame bright-field laser schlieren/shadowgraphy imaging system was used to image the window opening dynamics on microsecond timescales. The imaging system is capable of achieving temporal resolution as low as tens of nanoseconds, which could be useful for imaging future targets/experiments with faster predicted opening timescales. This system used a Coherent Verdi 6-W continuous-wave (CW) laser source with a 532-nm wavelength. A laser-fiber coupler was used to transport the beam from the laser room to the experiment. The optical setup included an achromat lens to collimate the diverging light rays as they exited the fiber, multiple mirrors to direct the collimated beam along the optical breadboard and through the target, and a focusing lens for relaying the light to the imaging detector. The focal length and position of the focusing lens were selected such that a negative image (a dark image on a bright background) would be formed from light rays that were refracted out of the optical system by the various target materials and escaping gas. Note that absorption and reflection processes also contribute to these negative images. Further note that our system did not use a dedicated schlieren aperture (small pinhole) at the focal point of the unperturbed laser (nor was a beam stop or knife edge used, since our system is bright-field schlieren/shadowgraphy). However, there is an effective schlieren aperture set by the acceptance angle  $\Delta\phi$  of the collection optics, which is  $1.46^\circ$  for our system. This acceptance angle determines the minimum average density gradient  $\nabla n$  that can be observed with our system. The angle is measured relative to the optical axis, and it describes the light cone that is maximally scattered by the target while

still being collected by the focusing lens, L, in Fig. 5. If a light ray (scattered or unscattered) is collected by the focusing lens in Fig. 5, then it does not contribute to a dark image on a bright background field. Only light rays scattered to an angle exceeding  $\Delta\phi = 1.46^\circ$  contribute to a dark image on a bright background field. Assuming a Gladstone-Dale constant  $K_n = 1.14 \times 10^{-23} \text{ cm}^3$  and an interaction distance  $D = 0.52 \text{ cm}$  through the column of escaping gas above the target, the minimum average density gradient that the system can detect/image is  $\nabla n \sim \Delta\phi/(DK_n) \sim 4.3 \times 10^{21} \text{ cm}^{-4}$ . In future experiments, an aperture, beam stop, or knife edge could be used to reduce  $\Delta\phi$  and thus measure finer density gradients. However, it is important to note that if  $\Delta\phi$  is reduced too much, then the spatial resolution of the overall imaging system could become diffraction limited. For the system used in these experiments, the overall spatial resolution of about  $22 \mu\text{m}$  (determined by the pixel resolution of the imaging detector) was not impacted by the system's diffraction limit, which was  $d \approx \lambda/[2 \sin(\Delta\phi)] \approx 10 \mu\text{m}$ , where  $\lambda = 532 \text{ nm}$  is the laser wavelength.

The schlieren/shadowgraphy images were recorded using a fast 12-frame ICCD camera (Invisible Vision<sup>®</sup> Ultra UHSi). For target alignment purposes, a laser power of 0.01 W was sufficient for a 100- $\mu\text{s}$  exposure when the ICCD gain was set to 90.

#### IV. EXPERIMENTAL RESULTS

Example iPhone images of the window opening dynamics are shown in Fig. 7. The 0-ms frame was chosen as the last frame with no window movement. From these images, it is clear that the window material opens upwards and out of what would be the preheating laser path in a MagLIF experiment. Additionally, the window opened as if it had hinged along the side where the window was not in contact with the wire (as intended); however, the window material also completely detached from the target, which was not anticipated. Furthermore, the bending of the nichrome wire into what would be the preheating laser path of a MagLIF experiment was not anticipated.

The iPhone diagnostic was useful for demonstrating proof-of-concept, but with a 4-ms time resolution, there were many unanswered questions, including how cleanly the window opened, how fast the window opened, and how fast the nichrome wire moved into the preheating laser path. To address these questions, the bright-field laser schlieren/shadowgraphy imaging system was implemented.

Example schlieren/shadowgraphy images of the window opening dynamics, on a microsecond timescale, are presented in Fig. 8. For this experiment, the target was filled to  $\Delta P = 27 \text{ psi}$ , the laser power was set to 0.03 W, the ICCD gain was set to 100, and the duration of the exposure for each frame was set to 10  $\mu\text{s}$ . The images were false colored to enhance contrast and to represent

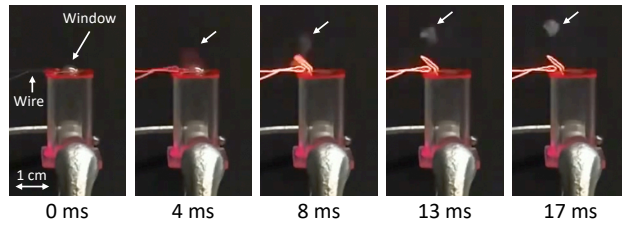


FIG. 7. Photographs (video frames) of an LEH window opening up and out of what would be the preheating laser path in a MagLIF experiment. The white arrow points to LEH window material as it moves. The nichrome wire glows red-hot as the electrical current heats the wire and melts/weakens the window. The temporal resolution is limited by the frame rate (240 fps) of the iPhone video camera that was used to acquire these images.

the green laser (532 nm) used to backlight the experiment. The preshot was taken before the experiment, and the  $t = 0 - 10 \mu\text{s}$  frame corresponds to the beginning of the current pulse shown in Fig. 6.

In the earlier images of Fig. 8, the window appears to push open along a hinge on the left side of the LEH perimeter. This is consistent with the fact that the open ends of the nichrome wire extend off to the left in these images—i.e., in these images, the wire is not in contact with the window material along the left side of the LEH perimeter. Additionally, the window hinges open to a fully upright position at  $t \approx 20 \mu\text{s}$ , which agrees well with the estimate from Eq. 1 ( $\tau_{\text{open}} \approx 14.3 \mu\text{s}$ ).

In the later images of Fig. 8, the window appears to tear away from the target after hinging open. The tear appears to be clean (with no apparent debris), and the window remains intact. These are important observations because window debris could contaminate the fuel in MagLIF and lead to enhanced radiative losses.

There are three different LEH window movement regimes that can be analyzed from Fig. 8. The first is defined as window opening. This includes the first four frames, when the LEH window is pivoting about its hinge point on the target. The second regime includes the fourth, fifth, and sixth frames, where the mushroom cloud above the target is visible. The third regime includes the last four frames, when the window is moving along the escaping gas column. It is important to note that all of these frames from Fig. 8 take place before the third frame of Fig. 7, which is one reason why the schlieren/shadowgraphy system was implemented. Velocities during these three regimes can be estimated. The window opening velocity is about  $310 \pm 80 \text{ m/s}$ , calculated from the angular velocity of the window as it rotates open ( $0.06 \pm 0.02 \text{ rad}/\mu\text{s}$  with the radius of the rotating arm equal to the 5.2 mm diameter of the window). The velocity of the escaping gas jet, calculated using the top of the mushroom cloud, is about  $280 \pm 110 \text{ m/s}$ . The window's axial velocity as it moves along the escaping gas column is about  $90 \pm 30 \text{ m/s}$ , calculated from the

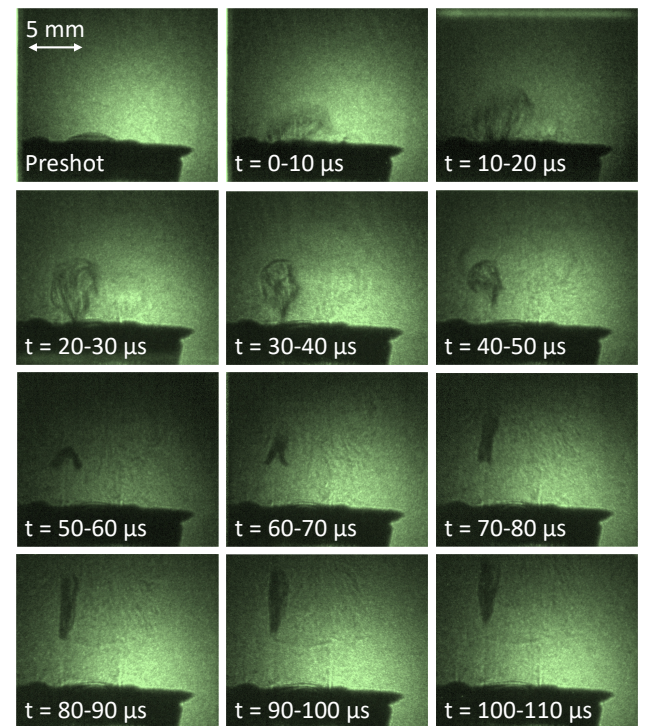


FIG. 8. Bright-field laser schlieren/shadowgraphy images of the LEH window opening up and out of what would be the preheating laser path in a MagLIF experiment. The largely intact window appears to ride along the edge of the escaping pressurized gas column.

motion of the bottom edge of the window in the last four frames of Fig. 8. This indicates that the velocities begin near the sound speed (343 m/s) and then decrease as the pressure inside of the target decreases. This slowing down as time advances and pressure decreases is also consistent with the window moving slowly in the last three frames of Fig. 7. The deceleration of the window at later times is likely caused by the ambient air pressure, drag on the window, and the window slipping out past the column of escaping gas into the ambient air. This further motivates conducting future experiments in vacuum conditions, where the window opening dynamics are expected to occur faster than the dynamics reported here.

Despite becoming detached from the target, the window never crosses what would be the preheating laser path in a MagLIF experiment. In fact, it appears that the detached window rides along the edge of the escaping gas column, which is also visible in the images of Fig. 8. Our original intent was for the LEH window to remain attached to the target at the hinge to prevent the window from inadvertently crossing the preheating laser path as a projectile. However, if the detached window rides along the edge of the escaping gas column in a predictable way, then crossing the preheating laser path may be less of a concern after all. Nevertheless, there is still a concern about the detached window interfering with other equip-

ment, such as diagnostics and the applied axial magnetic field coils used in MagLIF experiments.<sup>19</sup> Future experiments will be designed to assess these issues in particular. Potential solutions include optimizing the LEH window material, optimizing the heat delivery to smaller sections of the window's perimeter, and strengthening the window at the hinge point.

Finally, the images in Fig. 8 show that the nichrome wire remains in place for at least 100  $\mu$ s. Thus, the nichrome wire will not interfere with the preheating laser pulse in MagLIF, since MagLIF experiments are conducted on timescales of hundreds of nanoseconds.

## V. CONCLUSIONS AND FUTURE WORK

This article has demonstrated the proof-of-concept for a pulsed-power implementation of Laser Gate. This article has also demonstrated the development of an experimental platform to study Laser Gate dynamics in detail. This platform includes an in-house target fabrication process, a target gas-fill system, a small pulsed-power device, and a 12-frame bright-field laser schlieren/shadowgraphy imaging system. We have used this platform to image the LEH window opening up and out of what would be the preheating laser path in a MagLIF experiment on the timescales expected. The window appears to have opened cleanly (with no apparent debris) and remained intact. The nichrome wire was found to remain in place long enough for this Laser Gate implementation to be compatible with MagLIF experiments.

Consistent results were obtained from the three shots imaged by the iPhone camera and from the three shots imaged by the bright-field laser schlieren/shadowgraphy system. Across the six trials that were performed, the window opening dynamics remained similar. As in the images presented in Fig. 8, the windows spun or folded while continuing to ride along the edge of the escaping gas column. The ability to successfully fabricate targets capable of holding the desired gas pressure has impacted the number of shots taken. We are currently working to improve our target fabrication abilities to conduct more experiments and to better assess shot-to-shot variations.

Future experiments will test this implementation of Laser Gate at conditions more closely aligned with those of fully integrated MagLIF experiments on the Z facility. These plans include testing Laser Gate in vacuum and at higher target fill pressures. In these future experiments, if the window opens into vacuum, we would expect a more diffuse radial and axial expansion of escaping gas, rather than the distinct column of primarily axially escaping gas observed in Fig. 8. This should push the window even farther from what would be the MagLIF preheating laser path, allowing the preheat laser to enter the target uninhibited by LEH window material. Experimental verification will be needed to assess when the window is sufficiently out of the laser path. This could be done by rotating the target by 90° to look through the LEH with

our laser imaging system. With experiments conducted in vacuum, we also expect a faster opening time since there will be less resistance as the window opens into vacuum. The higher fill pressures can be achieved by using beveled washers and a smaller radius LEH to match the  $(\delta/r)^2$  value of the SNL targets. Both of these changes are expected to make the window open even faster than the results presented in this paper—though these predictions must be validated experimentally. In these future experiments, an interferometry system will be used to quantify the density and total mass of the escaping gas column, and laser-probing techniques (e.g., laser-induced fluorescence) will be used to study the rarefaction wave that propagates down into the transparent target. We are also redesigning and rebuilding hardware for integration into various testing facilities at SNL. These plans include testing helium and deuterium as target fill gases. With future improvements, we hope to eventually integrate the Laser Gate concept into full-scale MagLIF experiments.

## ACKNOWLEDGEMENTS

This work was supported by the NNSA Laboratory Residency Graduate Fellowship under DOE contract DE-NA-0003864, the NNSA Stewardship Sciences Academic Program under DOE cooperative agreement DE-NA-0003764, the NNSA-DS/SC-OFES HEDLP Program under DOE contract DE-NA-0002956, and by Sandia National Laboratories, a multi-mission laboratory managed and operated by National Technology and Engineering Solutions of Sandia, LLC., a wholly owned subsidiary of Honeywell International, Inc., for the U.S. Department of Energy's National Nuclear Security Administration under contract DE-NA-0003525.

## DATA AVAILABILITY

The data that supports the findings of this study are available within the article.

<sup>1</sup>S. A. Slutz, M. C. Herrmann, R. A. Vesey, A. B. Sefkow, D. B. Sinars, D. C. Rovang, K. J. Peterson, and M. E. Cuneo, *Physics of Plasmas* **17**, 056303 (2010), <https://doi.org/10.1063/1.3333505>.

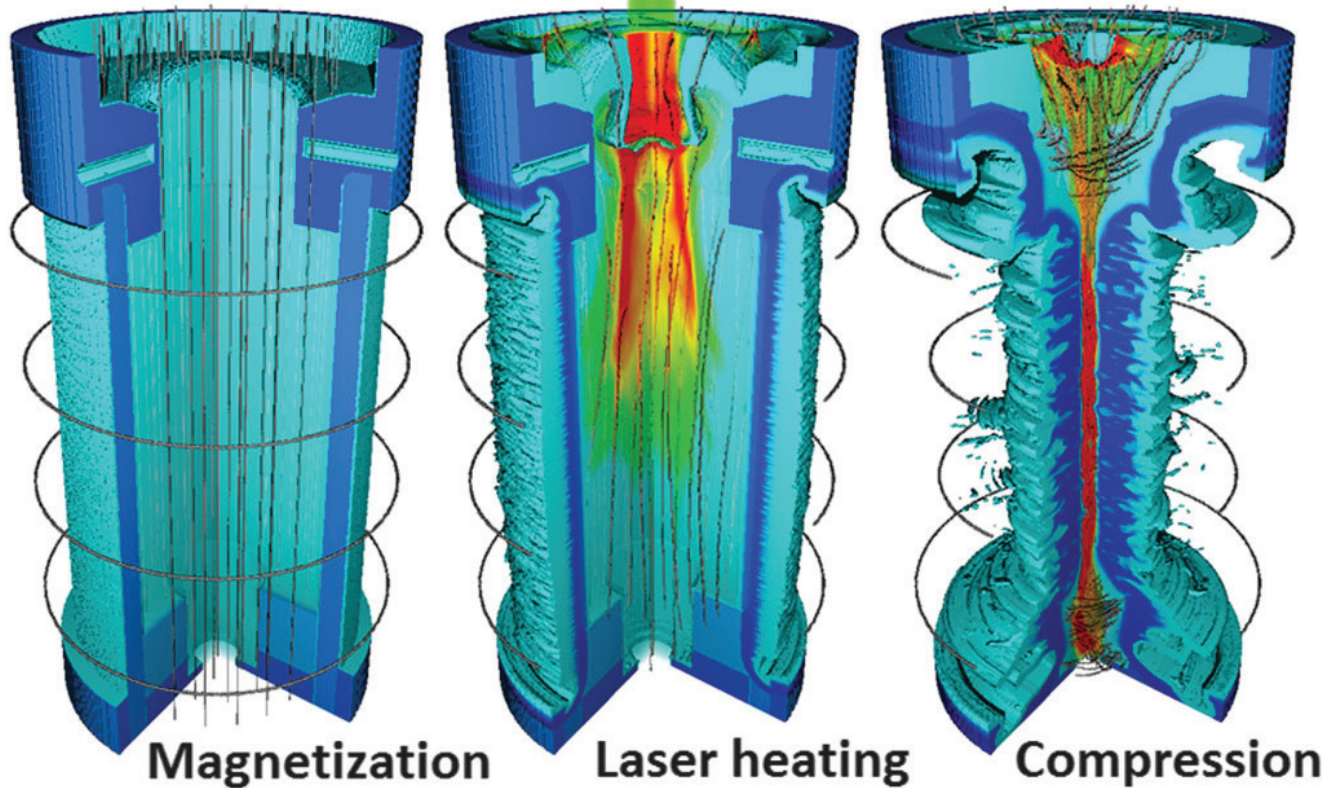
<sup>2</sup>M. E. Cuneo, M. C. Herrmann, D. B. Sinars, S. A. Slutz, W. A. Stygar, R. A. Vesey, A. B. Sefkow, G. A. Rochau, G. A. Chandler, J. E. Bailey, J. L. Porter, R. D. McBride, D. C. Rovang, M. G. Mazarakis, E. P. Yu, D. C. Lampa, K. J. Peterson, C. Nakhleh, S. B. Hansen, A. J. Lopez, M. E. Savage, C. A. Jennings, M. R. Martin, R. W. Lemke, B. W. Atherton, I. C. Smith, P. K. Rambo, M. Jones, M. R. Lopez, P. J. Christenson, M. A. Sweeney, B. Jones, L. A. McPherson, E. Harding, M. R. Gomez, P. F. Knapp, T. J. Awe, R. J. Leeper, C. L. Ruiz, G. W. Cooper, K. D. Hahn, J. McKenney, A. C. Owen, G. R. McKee, G. T. Leifeste, D. J. Ampleford, E. M. Waisman, A. Harvey-Thompson, R. J. Kaye, M. H. Hess, S. E. Rosenthal, and M. K. Matzen, *IEEE Transactions on Plasma Science* **40**, 3222 (2012).

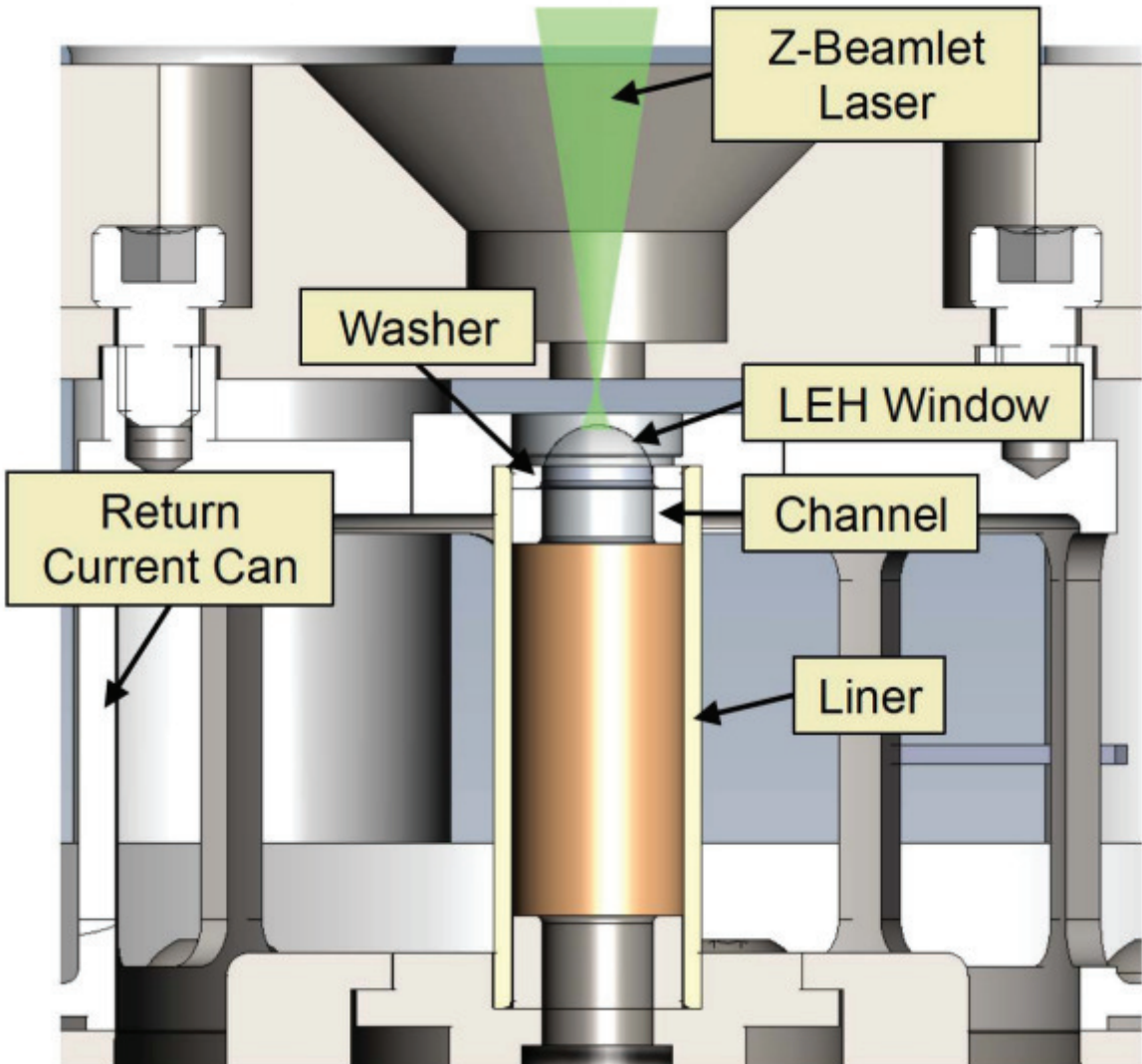
<sup>3</sup>M. R. Gomez, S. A. Slutz, A. B. Sefkow, D. B. Sinars, K. D. Hahn, S. B. Hansen, E. C. Harding, P. F. Knapp, P. F. Schmit,

This is the author's peer reviewed, accepted manuscript. However, the online version of record will be different from this version once it has been copyedited and typeset.

PLEASE CITE THIS ARTICLE AS DOI:10.1063/1.5139663

- C. A. Jennings, T. J. Awe, M. Geissel, D. C. Rovang, G. A. Chandler, G. W. Cooper, M. E. Cuneo, A. J. Harvey-Thompson, M. C. Herrmann, M. H. Hess, O. Johns, D. C. Lamppa, M. R. Martin, R. D. McBride, K. J. Peterson, J. L. Porter, G. K. Robertson, G. A. Rochau, C. L. Ruiz, M. E. Savage, I. C. Smith, W. A. Stygar, and R. A. Vesey, *Phys. Rev. Lett.* **113**, 155003 (2014).
- <sup>4</sup>S. A. Slutz, M. R. Gomez, S. B. Hansen, E. C. Harding, B. T. Hutsel, P. F. Knapp, D. C. Lamppa, T. J. Awe, D. J. Ampleford, D. E. Bliss, G. A. Chandler, M. E. Cuneo, M. Geissel, M. E. Glinsky, A. J. Harvey-Thompson, M. H. Hess, C. A. Jennings, B. Jones, G. R. Laity, M. R. Martin, K. J. Peterson, J. L. Porter, P. K. Rambo, G. A. Rochau, C. L. Ruiz, M. E. Savage, J. Schwarz, P. F. Schmit, G. Shipley, D. B. Sinars, I. C. Smith, R. A. Vesey, and M. R. Weis, *Physics of Plasmas* **25**, 112706 (2018), <https://doi.org/10.1063/1.5054317>.
- <sup>5</sup>M. R. Gomez, S. A. Slutz, P. F. Knapp, K. D. Hahn, M. R. Weis, E. C. Harding, M. Geissel, J. R. Fein, M. E. Glinsky, S. B. Hansen, A. J. Harvey-Thompson, C. A. Jennings, I. C. Smith, D. Woodbury, D. J. Ampleford, T. J. Awe, G. A. Chandler, M. H. Hess, D. C. Lamppa, C. E. Myers, C. L. Ruiz, A. B. Sefkow, J. Schwarz, D. A. Yager-Elorriaga, B. Jones, J. L. Porter, K. J. Peterson, R. D. McBride, G. A. Rochau, and D. B. Sinars, *IEEE Transactions on Plasma Science* **47**, 2081 (2019).
- <sup>6</sup>P. F. Knapp, M. R. Gomez, S. B. Hansen, M. E. Glinsky, C. A. Jennings, S. A. Slutz, E. C. Harding, K. D. Hahn, M. R. Weis, M. Evans, M. R. Martin, A. J. Harvey-Thompson, M. Geissel, I. C. Smith, D. E. Ruiz, K. J. Peterson, B. M. Jones, J. Schwarz, G. A. Rochau, D. B. Sinars, R. D. McBride, and P.-A. Gourdain, *Physics of Plasmas* **26**, 012704 (2019), <https://doi.org/10.1063/1.5064548>.
- <sup>7</sup>M. Geissel, A. J. Harvey-Thompson, T. J. Awe, D. E. Bliss, M. E. Glinsky, M. R. Gomez, E. Harding, S. B. Hansen, C. Jennings, M. W. Kimmel, P. Knapp, S. M. Lewis, K. Peterson, M. Schollmeier, J. Schwarz, J. E. Shores, S. A. Slutz, D. B. Sinars, I. C. Smith, C. S. Speas, R. A. Vesey, M. R. Weis, and J. L. Porter, *Physics of Plasmas* **25**, 022706 (2018), <https://doi.org/10.1063/1.5003038>.
- <sup>8</sup>A. Dunaevsky, A. Goltsov, J. Greenberg, E. Valeo, and N. J. Fisch, *Physics of Plasmas* **13**, 043106 (2006), <https://doi.org/10.1063/1.2195383>.
- <sup>9</sup>A. J. Harvey-Thompson, M. Geissel, C. A. Jennings, M. R. Weis, M. R. Gomez, J. R. Fein, D. J. Ampleford, G. A. Chandler, M. E. Glinsky, K. D. Hahn, S. B. Hansen, E. C. Harding, P. F. Knapp, R. R. Paguio, L. Perea, K. J. Peterson, J. L. Porter, P. K. Rambo, G. K. Robertson, G. A. Rochau, C. L. Ruiz, J. Schwarz, J. E. Shores, D. B. Sinars, S. A. Slutz, G. E. Smith, I. C. Smith, C. S. Speas, K. Whittemore, and D. Woodbury, *Physics of Plasmas* **26**, 032707 (2019), <https://doi.org/10.1063/1.5086044>.
- <sup>10</sup>J. R. Davies, R. E. Bahr, D. H. Barnak, R. Betti, M. J. Bonino, E. M. Campbell, E. C. Hansen, D. R. Harding, J. L. Peebles, A. B. Sefkow, W. Seka, P.-Y. Chang, M. Geissel, and A. J. Harvey-Thompson, *Physics of Plasmas* **25**, 062704 (2018), <https://doi.org/10.1063/1.5030107>.
- <sup>11</sup>B. Galloway, personal communication (2019).
- <sup>12</sup>S. W. Haan, P. A. Amendt, D. A. Callahan, T. R. Dittrich, M. J. Edwards, B. A. Hammel, D. D. Ho, O. S. Jones, J. D. Lindl, M. M. Marinak, D. H. Munro, S. M. Pollaine, J. D. Salmonson, B. K. Spears, and L. J. Suter, *Fusion Science and Technology* **51**, 509 (2007), <https://doi.org/10.13182/FST51-509>.
- <sup>13</sup>B. Lairson, R. Smith, J. Guckian, T. Ayers, and S. Bhandarkar, *Fusion Science and Technology* **59**, 262 (2011), <https://doi.org/10.13182/FST10-3686>.
- <sup>14</sup>M. R. Gomez, S. A. Slutz, A. B. Sefkow, K. D. Hahn, S. B. Hansen, P. F. Knapp, P. F. Schmit, C. L. Ruiz, D. B. Sinars, E. C. Harding, C. A. Jennings, T. J. Awe, M. Geissel, D. C. Rovang, I. C. Smith, G. A. Chandler, G. W. Cooper, M. E. Cuneo, A. J. Harvey-Thompson, M. C. Herrmann, M. H. Hess, D. C. Lamppa, M. R. Martin, R. D. McBride, K. J. Peterson, J. L. Porter, G. A. Rochau, M. E. Savage, D. G. Schroen, W. A. Stygar, and R. A. Vesey, *Physics of Plasmas* **22**, 056306 (2015), <https://aip.scitation.org/doi/pdf/10.1063/1.4919394>.
- <sup>15</sup>A. Harvey-Thompson, personal communication (2019).
- <sup>16</sup>S. A. Slutz and R. A. Vesey, *Phys. Rev. Lett.* **108**, 025003 (2012).
- <sup>17</sup>A. M. Steiner, *The Electrothermal Instability on Pulsed Power Ablations of Thin Foils*, Ph.D. thesis, University of Michigan (2016).
- <sup>18</sup>A. M. Steiner, P. C. Campbell, D. A. Yager-Elorriaga, N. M. Jordan, R. D. McBride, Y. Y. Lau, and R. M. Gilgenbach, *IEEE Transactions on Plasma Science* **46**, 3753 (2018).
- <sup>19</sup>D. C. Rovang, D. C. Lamppa, M. E. Cuneo, A. C. Owen, J. McKenney, D. W. Johnson, S. Radovich, R. J. Kaye, R. D. McBride, C. S. Alexander, T. J. Awe, S. A. Slutz, A. B. Sefkow, T. A. Hail, P. A. Jones, J. W. Argo, D. G. Dalton, G. K. Robertson, E. M. Waisman, D. B. Sinars, J. Meissner, M. Milhous, D. N. Nguyen, and C. H. Mielke, *Rev. Sci. Instrum.* **85**, 124701 (2014).





LEH window

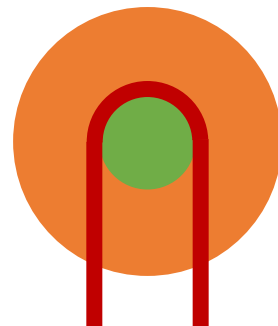
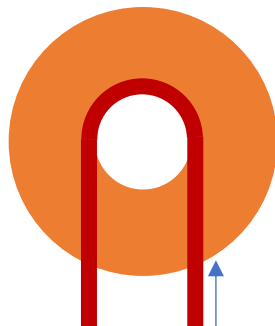
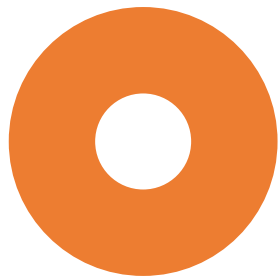
Wrap wire around LEH

Run current through wire

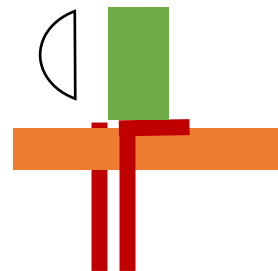
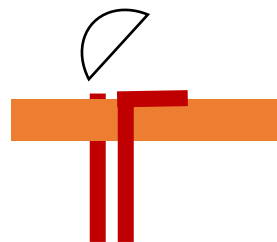
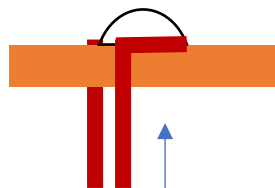
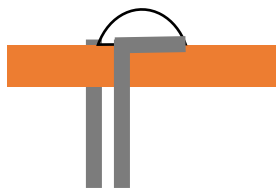
Wire heats and window opens

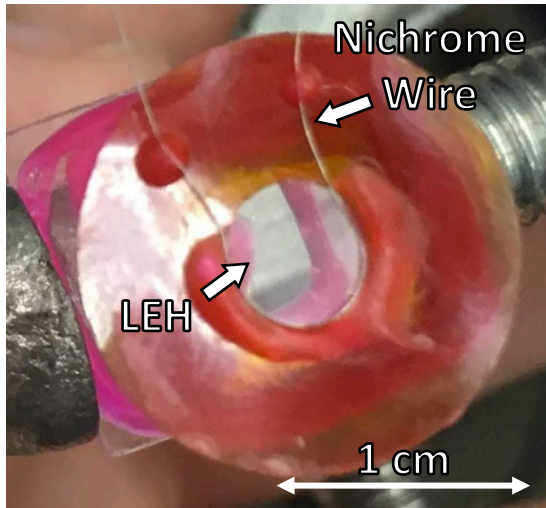
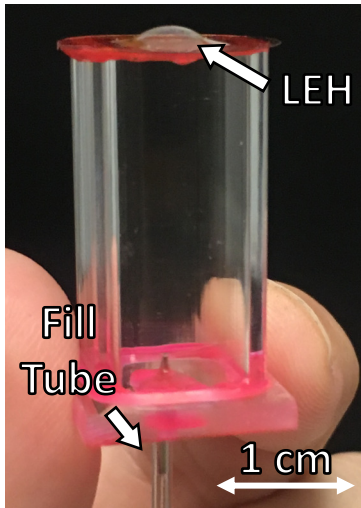
Laser enters

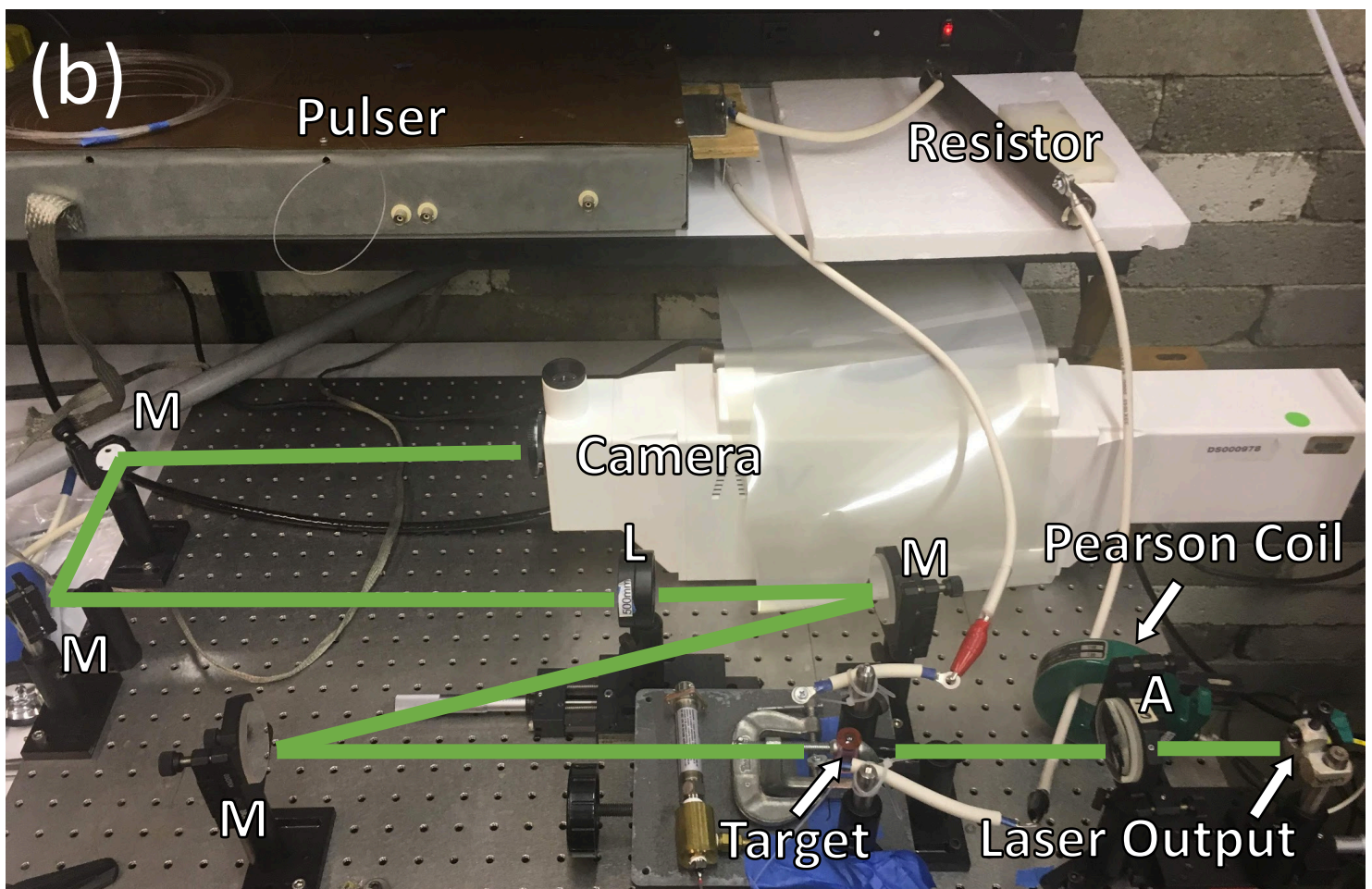
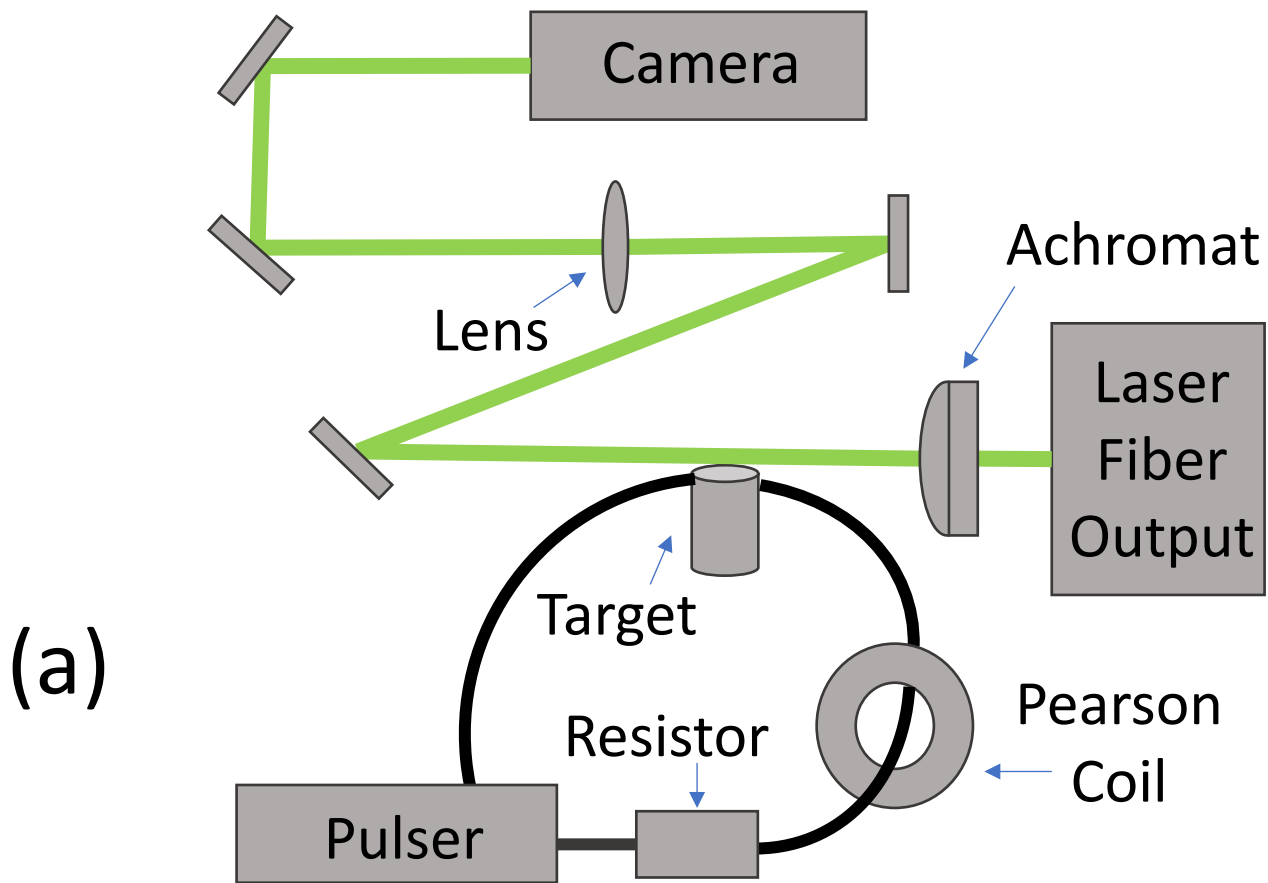
Top down



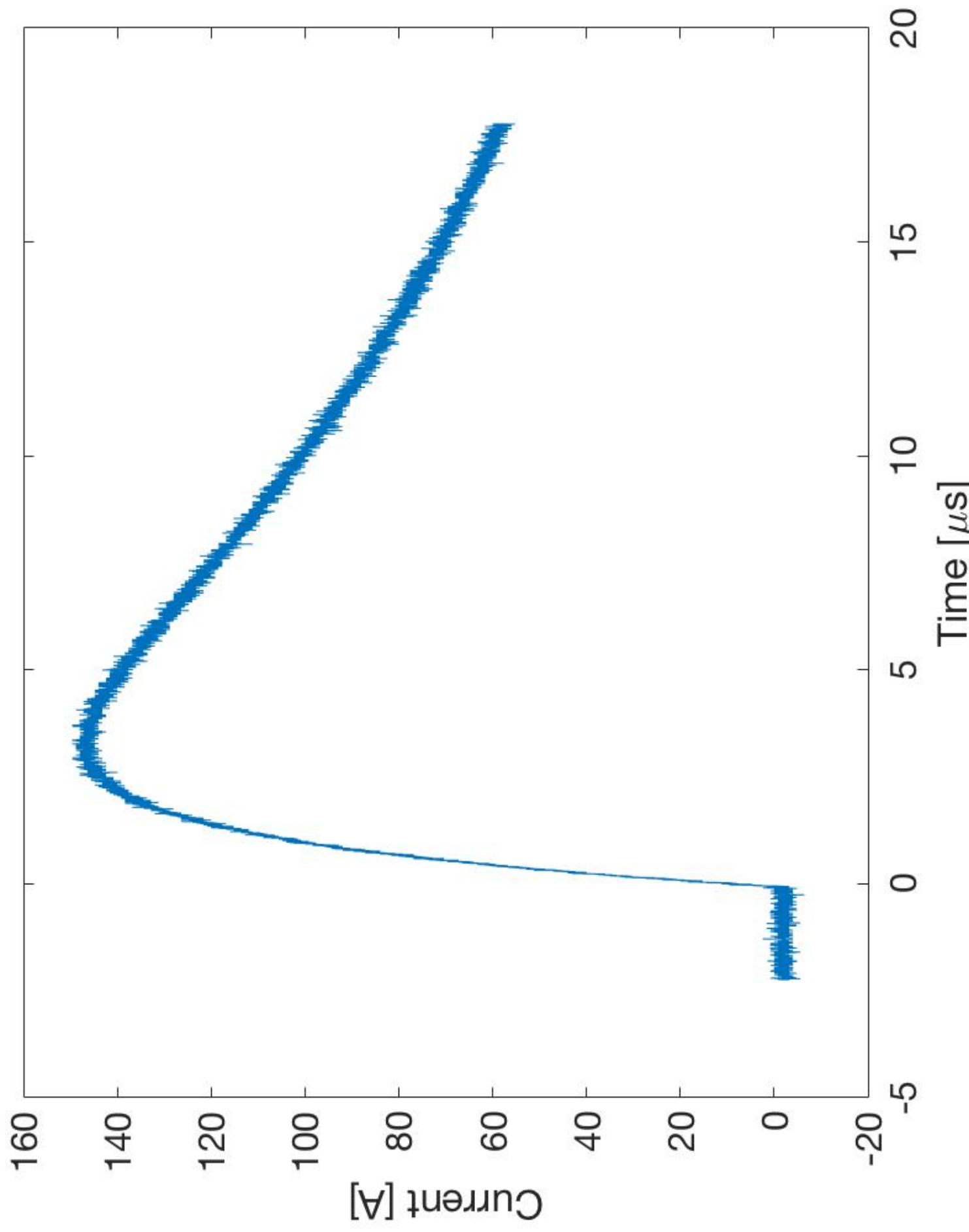
Side on

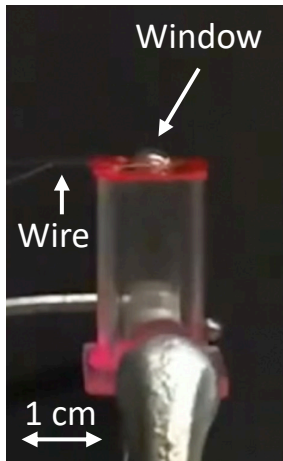




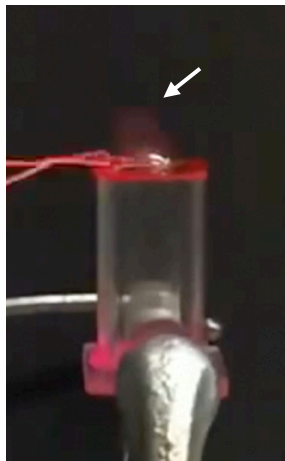


This is the author's peer reviewed, accepted manuscript. However, the online version of record will be different from this version once it has been copyedited and typeset.  
PLEASE CITE THIS ARTICLE AS DOI:10.1063/1.5139663

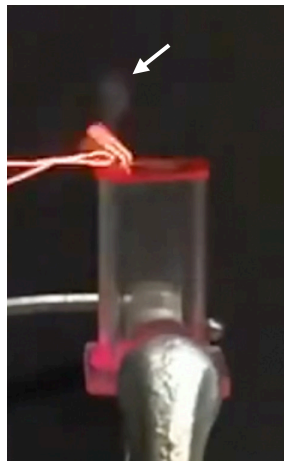




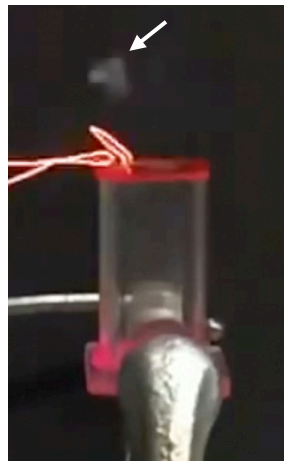
0 ms



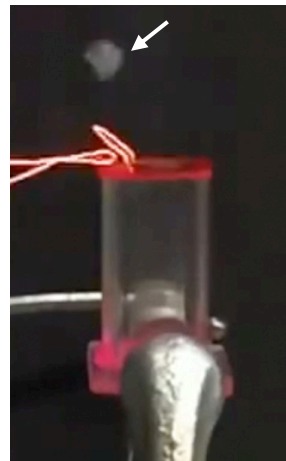
4 ms



8 ms



13 ms



17 ms

